JOURNAL OF PLANKTON RESEARCH | VOLUME 32 | NUMBER 1 | PAGES 1–14 | 2010

General patterns in the size scaling of phytoplankton abundance in coastal waters during a 10-year time series

MARÍA HUETE-ORTEGA[1]*, EMILIO MARAÑÓN[1], MANUEL VARELA[2] AND ANTONIO BODE[2]

[1]DEPARTAMENTO DE ECOLOGÍA Y BIOLOGÍA ANIMAL, FACULTAD DE CIENCIAS DEL MAR, UNIVERSIDAD DE VIGO, 36310 VIGO, SPAIN AND [2]INSTITUTO ESPAÑOL DE OCEANOGRAFÍA, CENTRO OCEANOGRÁFICO DE A CORUÑA, APDO. 130, 15080 A CORUÑA, SPAIN

*CORRESPONDING AUTHOR: mhuete@uvigo.es

Received June 4, 2009; accepted in principle September 29, 2009; accepted for publication October 2, 2009

Corresponding editor: William Li

To ascertain the general patterns in phytoplankton size structure of a temperate, coastal ecosystem, we determined the scaling relationship between total abundance and cell size (size spectrum) for nano- and micro-phytoplankton in a shelf station off NW Iberian Peninsula on a monthly basis during the period 1993–2002. The inverse linear relationship between log abundance and log cell size was persistent throughout the water column and across seasonal and inter-annual time scales. In addition, and despite the high productivity and marked temporal variability in water column structure at our study site, departures from linearity in the size spectra were rare. The slope (−0.96) of the overall size spectrum for the entire time series indicated that roughly equal amounts of biomass were present over different logarithmic size classes in the size range considered. The phytoplankton size spectra had similar average slopes during winter mixing, early upwelling, summer stratification and autumn downwelling, suggesting that, under these oceanographic conditions, both nano- and micro-phytoplankton respond similarly to environmental variability. In contrast, significantly less negative slopes were observed during upwelling relaxation, indicating an increased importance of larger cells. Our results illustrate the utility of individual size distributions to provide a synthetic description of phytoplankton community structure in dynamic, non steady-state marine ecosystems.

INTRODUCTION

Phytoplankton size structure is of critical importance for the functioning of pelagic ecosystems both from an ecological and a biogeochemical point of view (Kiørboe, 1993; Legendre and Rassoulzadegan, 1996; Marañón, 2009). When small cells account for the bulk of phytoplankton biomass, as is typically the case in oligotrophic waters, sedimentation rates are small, a complex microbial food web dominates the cycling of matter and the potential for downward carbon export is reduced (microbial loop; Azam *et al.*, 1983). When large cells dominate the community, sedimentation losses are higher and most of the primary production is channelled through short food chains, resulting in an increased efficiency of the biological pump in transporting carbon towards deep layers (classical food web; Cushing, 1989).

Given that body size affects all aspects of the biology of organisms, including lifespan, home range size, metabolic rates and resource use (Peters, 1983; Brown *et al.*, 2004), the relationship between body size and abundance has long been recognized as a fundamental property of communities and ecosystems. One of the most widely used approaches to study this relationship in aquatic ecosystems is to construct an individual size

doi:10.1093/plankt/fbp104, available online at www.plankt.oxfordjournals.org. Advance Access publication 28 October, 2009

distribution, also known as size spectrum (White *et al.*, 2007). In this distribution, the total abundance or biomass of all individuals within each logarithmic size class, irrespective of species, is plotted against the nominal or mean cell size of each size class (Sheldon *et al.*, 1972; Rodríguez and Mullin, 1986; Sprules and Munawar, 1986; Rodríguez *et al.*, 2001).

When the size spectrum is constructed using total abundance (N), the resulting distribution usually follows a simple decreasing power function of cell size (M) such that $N \propto M^b$, where b is the size scaling exponent. Logarithmic transformation yields $\log N = a + b \log M$, where a and b are the intercept and slope, respectively, of the linear relationship. The value of b, which typically takes values between -1.3 and -0.6, can be regarded as a synthetic descriptor of the phytoplankton community size structure. Typically, unproductive ecosystems are characterized by more negative b values (-1.3 to -1.1), whereas productive waters show less negative b values (-0.8 to -0.6) (Cavender-Bares *et al.*, 2001; Reul *et al.*, 2005; Marañón *et al.*, 2007). In addition, it has been shown that more productive ecosystems that are also subject to stronger hydrodynamical forcing can show irregularities (i.e. nonlinearities) in the size spectrum (Sprules and Munawar, 1986; Reul *et al.*, 2006), resulting from the accumulation of a small number of species.

Despite the fact that the relationship between water column structure and phytoplankton size spectra has been studied for decades, most previous analyses either did not consider seasonal variability or were based on a small number of observations conducted during just 1 year. Thus, the emphasis has been placed mostly on the relationship between particular hydrodynamic events and the resulting changes in phytoplankton size structure (Rodríguez *et al.*, 1987; Reul *et al.*, 2005, 2006) rather than in the search of broader patterns across a range of temporal scales. The present study uses a large set of monthly data of phytoplankton composition and abundance collected at a shelf station off A Coruña (NW Iberian Peninsula) during 1993–2002. The region is characterized by the typical seasonal variability of coastal temperate seas and, in addition, is subject to intermittent upwelling pulses during the period April–September (Fraga, 1981; Casas *et al.*, 1997; Teira *et al.*, 2003), thus leading to a particularly dynamic pelagic ecosystem. Our main objectives here are (i) to verify the validity of the power-law relationship between phytoplankton cell size and abundance to describe phytoplankton size structure in a non-steady-state ecosystem; (ii) to describe the seasonal and interannual variability in phytoplankton size structure; and (iii) to obtain general patterns in the size scaling of phytoplankton abundance in relation to contrasting hydrographic conditions.

METHOD

Sampling

The data used in the present study were obtained within the framework of the time-series project RADIALES, conducted by the Instituto Español de Oceanografía in the Ría of A Coruña (NW Spain) (Valdés *et al.*, 2002). This project involves a monthly sampling of 5 stations along a coast-ocean transect and has been running since 1989. Our analysis is focused on the abundance and cell size of phytoplankton collected at the station 2 (depth = 80 m; 43°25′30″N, 08°26′20″W; Fig. 1) during the period January 1993–December 2002. On each sampling visit, the vertical distribution of temperature and salinity was measured with a CTD SBE-25 probe. Water samples were collected with 5 L Niskin bottles or a rosette sampler from depths of 0, 5, 10, 20, 30 and 40 m. For each sampling depth, samples were collected for the determination of nutrient concentration, chlorophyll *a* (Chl *a*) concentration and phytoplankton abundance following the methods previously reported in Casas *et al.* (Casas *et al.*, 1997, 1999) and Teira *et al.* (Teira *et al.*, 2003). In addition, the daily averaged Ekman offshore transport of surface water across a transect parallel to the shoreline was estimated as described by Lavin *et al.* (Lavin *et al.*, 1991), using wind speed and direction data measured every 6 h at the Centro Meteorológico Zonal of A Coruña (Agencia Estatal de Meteorología). The sign and value of this transport are used as indicative of the occurrence and intensity of the upwelling events, respectively, as positive values indicate upwelling-favourable, offshore Ekman transport, whereas negative values indicate downwelling-favourable, onshore Ekman transport. Water-column stability was estimated using the Brunt–Väisalä frequency (N) calculated from the density difference between 0 and 40 m depth:

$$N = \left[\frac{4g(\sigma_2 - \sigma_1)}{(\sigma_2 + \sigma_1)\ (z_2 - z_1)}\right]^{1/2}$$

where g is the acceleration gravity value, σ_2 and σ_1 are the densities at 40 and 0 m, respectively, and z_2 and z_1 are the sampling depths.

Phytoplankton abundance and cell size

Phytoplankton samples of volume 50–100 mL were preserved in Lugol's solution and kept in the dark until analysis. Samples were always counted by the same person using a Nikon Diaphot TMD microscope from 1993 to May 1997 and a Nikon Eclipse TE300

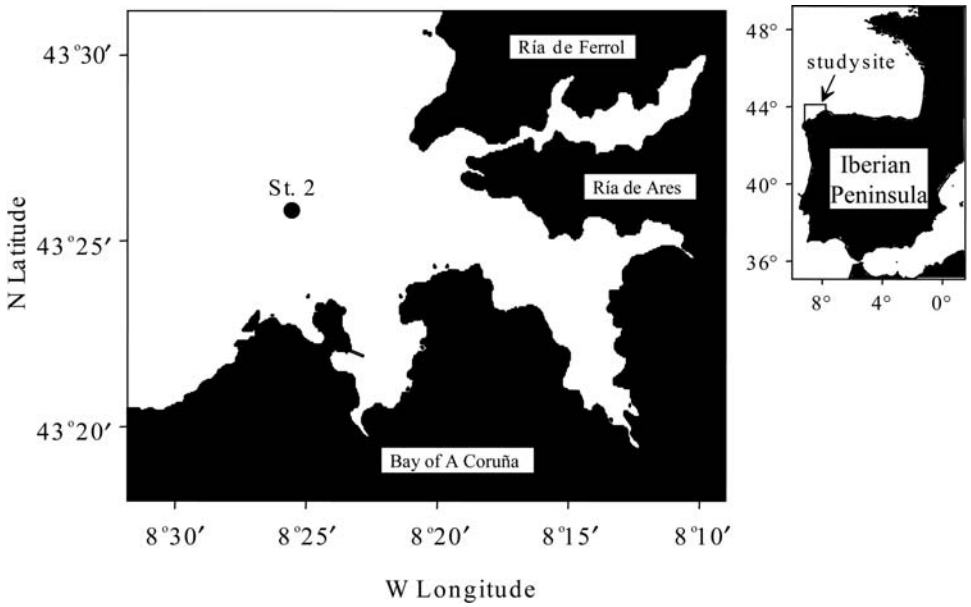

Fig. 1. Map of the sampling site off A Coruña Shelf (NW Iberian peninsula).

microscope from June 1997 to the end of the time series, following the technique described by Utermöhl (Lund *et al.*, 1958). A magnification of 100× was used for large forms, 250× for intermediate forms and 400× and 1000× for microflagellates. Whenever possible, organisms were classified at the species or genus level. Cell biovolume for each species was estimated in some samples from measurements of cell dimensions under the microscope, assigning a certain geometric shape to each species (Edler, 1979), and in the case of colonial species, only the cell size and the cell abundance were considered. An average cell size obtained from these measurements was used in subsequent analysis. For those species or genera for which no cell size measurements were available, cell volume was taken from the literature. The cell size range considered in our analysis was the nano- and micro-phytoplankton [2–20 and >20 μm of equivalent spherical diameter (ESD), respectively]. The total number of phytoplankton samples analysed for the present study was 571.

Size–abundance spectra

Size–abundance spectra were constructed using the phytoplankton abundance and cell size data. Size classes were established on an octave ($\log_2$) scale of biovolume and total cell abundance was calculated for each class by summing the abundance of all species included in it. The maximum number of size classes obtained was 19, ranging from 2 to ∼200 μm of ESD. Afterwards, the $\log_{10}$ of total abundance was plotted against the $\log_{10}$ of the lower limit of the corresponding octave size class in order to obtain a linear relationship (Blanco *et al.*, 1994; Reul *et al.*, 2005). Given that methodological error was present in both variables, a Model II regression analysis by the reduced major-axis method was carried out for each spectrum in order to estimate the regression slope and the *Y*-intercept (Laws and Archie, 1981). When a comparison between spectral slope values was necessary, Student's *t*-test following the Clarke method was used (Clarke, 1980). Size–abundance spectra with a determination coefficient (r^2) lower than 0.5 (less than 15% of all spectra) were eliminated and discarded from further analysis.

In order to analyse the phytoplankton size structure along the whole time series, we obtained size–abundance spectra at different levels of integration. At a first level, we constructed the size–abundance spectra for each month and sampling depth, obtaining approximately 600 spectra. In addition, data from the different sampling depths on each month were pooled together, thus yielding a size–abundance spectrum for the whole water column, hereafter referred to as water column macrospectra. These macrospectra result from plotting together all the individual spectra obtained for a given sampling date. Reduced major axis (r.m.a.) regression was applied to these macrospectra with the object of verifying the existence of linearity in the size–abundance relationship. As explained above for the individual spectra, those macrospectra with a determination coefficient below 0.5 were not considered for further analysis. At a third level of integration, annual

macrospectra were also obtained, by plotting together all the water column macrospectra for each year. Finally, a single macrospectrum for the entire data set was also constructed by combining all annual macrospectra.

Time-series analysis

With the aim of analysing the interannual and seasonal variability in our data set, we carried out a Fourier analysis in order to assess the periodicity of the time series, and later the variables were broken down into different sources of variability such as the seasonality and the interannual trend or the residuals (Nogueira *et al.*, 1997). The variables subjected to time-series analysis were temperature, salinity, mixing layer depth, nutrient concentration, the size–abundance spectra slopes at 5 and 40 m depth, the water column macrospectra slopes, Ekman transport and the monthly values of the North Atlantic Oscillation index. Once variables were broken down, correlation coefficients between the sources identified were calculated and cross-correlation tests between them were carried out to assess the relationship between the abiotic factors (hydrographic variables and nutrient concentration) and phytoplankton community size structure. Although seasonal sources were obtained for some of those variables, our analysis was focused on the interannual variability of the data set. The level of significance of the identified interannual trends was tested by first-order regression analysis. Statistical analyses were made using MATLAB software (Component Run Time version 7.7).

RESULTS

Hydrography and Chl *a*

The hydrodynamic pattern at the sampling station was typical of the NW Iberian peninsula, which is highly influenced by the predominant winds in each period of the year. Thus, in autumn and winter, there is a clear dominance of downwelling, whereas in spring and summer upwelling pulses prevail (Fig. 2). In spring, the onset of vertical stratification, mainly as a result of surface water warming, favours the development of phytoplankton blooms (Fig. 3). In addition, sequences of upwelling–relaxation–downwelling events are frequent in summer, causing the advection of cold and nutrient-rich water into the photic layer and the development of summer blooms during the relaxation period.

In spite of its interannual variability, station 2 showed the characteristic seasonal patterns of temperate coastal ecosystems: low temperatures, high nitrate concentrations and low Chl *a* concentration during late autumn and winter, and warmer temperatures and higher Chl *a* concentrations during the rest of the year (Figs 3 and 4). Vertical mixing was evident from January until April, with temperatures around 13°C throughout the water column (Figs 3a and 4b). Warmer temperatures occurred during summer and early autumn, when thermal stratification was present, mainly in summertime (Fig. 3a). The highest temperatures, observed in early autumn, coincided with the intensification of downwelling events that cause the accumulation of shelf waters against the coast (Fig. 4b). In addition, the intense mixing of the water column in winter resulted in a vertically homogeneous distribution of nutrients. Conversely, during summer, nutrient concentrations increased with depth as a result of active phytoplankton consumption in the upper layers and the re-mineralization of sinking organic matter below the photic layer (Figs 3b and 4c). Finally, the seasonal pattern was also clearly observable in Chl *a* concentrations, with high values being measured during summer and lower values in winter (Figs 3c and 4d). Thus, the monthly averaged values of Chl *a* at 5 m depth ranged between 3.6 mg m^{-3} in June and 0.72 mg m^{-3} in January. The maximum values were observed in summer, coinciding with a moderate stratification of the water column and higher incident irradiances that favour the development of summer blooms after the enrichment of the photic layer by upwelling events (Fig. 4d).

Hydrographic periods

With the aim of analysing the seasonal variability of phytoplankton community size structure, we identified five hydrographic periods relevant to the phytoplankton succession during the annual cycle. This classification was based on the temporal variability of the following environmental factors: surface temperature, nitrate and Chl *a* concentrations, averaged Ekman transport over the 6 days prior to sampling date and water column stability estimated by the Brunt–Väisalä frequency (N).

The five hydrographic periods identified, whose characteristics, described in Table I, are similar to those previously reported for the study area (Casas *et al.*, 1997; Varela *et al.*, 2001), were: winter-mixing, upwelling type I (initial stage), upwelling type II (final stage), stratification and downwelling. The two types of upwelling periods identified differ mainly in nutrient and Chl *a* concentration. Upwelling I corresponds to the initial stages of the upwelling event, when nitrate concentration is higher and Chl *a* concentration is still

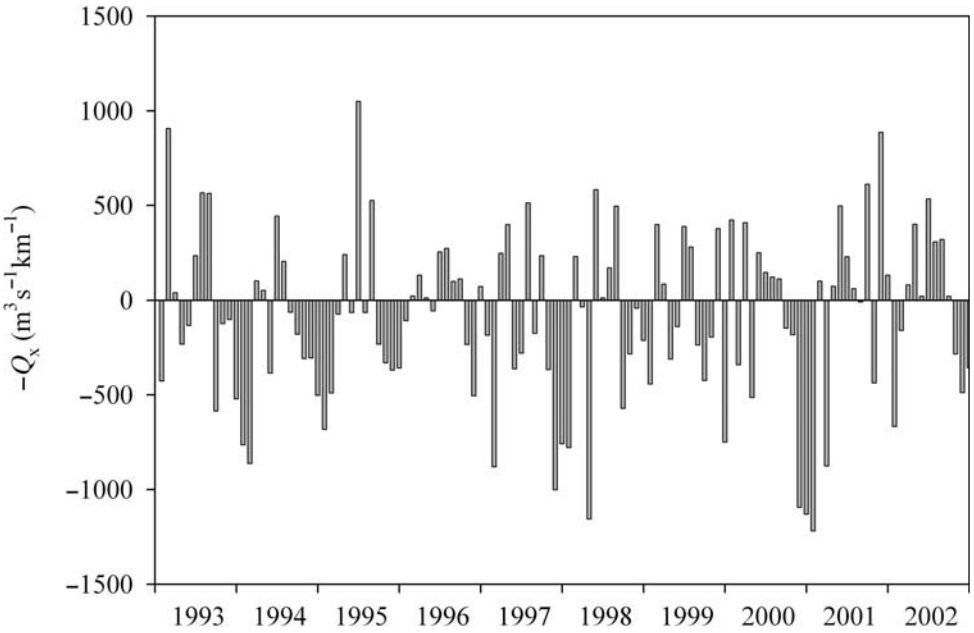

Fig. 2. Monthly averaged values of the Ekman transport ($m^3\ s^{-1}\ km^{-1}$) during the period of study. Positive and negative values of this index indicate upwelling-favourable and downwelling-favourable conditions, respectively.

relatively low. Upwelling type II corresponds to the final stages of upwelling events, when the northern winds relax and a moderate stratification of the water column leads to bloom development. The winter-mixing period shows the characteristics of temperate waters in late autumn and winter, with a high nutrient concentration, strong vertical mixing and low phytoplankton biomass. In contrast, the stratification period is characterized by a strong vertical thermal gradient and a high water-column stability. Finally, downwelling conditions are frequent in early autumn and involve the advection of warm water from the shelf towards the coast.

General size–abundance patterns

A significant, inverse linear relationship between abundance and cell size was persistent throughout the study and at different levels of integration, including (i) individual samples from a given depth, (ii) water-column spectra and (iii) annual spectra (Fig. 5). During the entire study period, the slope of the log–log relationship between phytoplankton total abundance and cell size in individual samples ranged from -1.39 to -0.66. In addition, we found that the slopes of the size–abundance spectra from different depths on the same sampling date were not significantly different from the slopes of the corresponding water column macrospectra (Clarke test always $P < 0.05$). Consequently, we assumed that the water-column macrospectra were representative of the phytoplankton community size structure for a given sampling date. Finally, when we pooled together all the observations collected for the whole time series, the resulting overall macrospectrum had a slope of -0.96 (Fig. 6).

Size–abundance spectra and hydrographic variability

Size–abundance macrospectra were obtained from each hydrographic period identified by plotting together all the water column macrospectra of the different sampling dates belonging to each period (Table II). All hydrographic periods showed similar values of the slope of the size–abundance relationship (Clarke test, $P > 0.05$) with the exception of upwelling II, which had a significantly less negative slope (Table II; Clarke test always $P < 0.0001$), indicating an increased importance of larger species. The intercept of the size–abundance macrospectra had its lowest value in winter, reflecting low levels of phytoplankton abundance, whereas the highest values were recorded during the upwelling type II and stratification periods (Table II).

We analysed the vertical variability in the size–abundance spectra during two contrasting hydrographic periods, winter mixing and stratification, by calculating the averaged slope of size–abundance spectra for each depth within each period (Fig. 7). During the winter-mixing period, the slope of the size–abundance spectra throughout the water column had very similar values, ranging between -0.95 and -1.02, reflecting the vertical homogeneity of phytoplankton community size

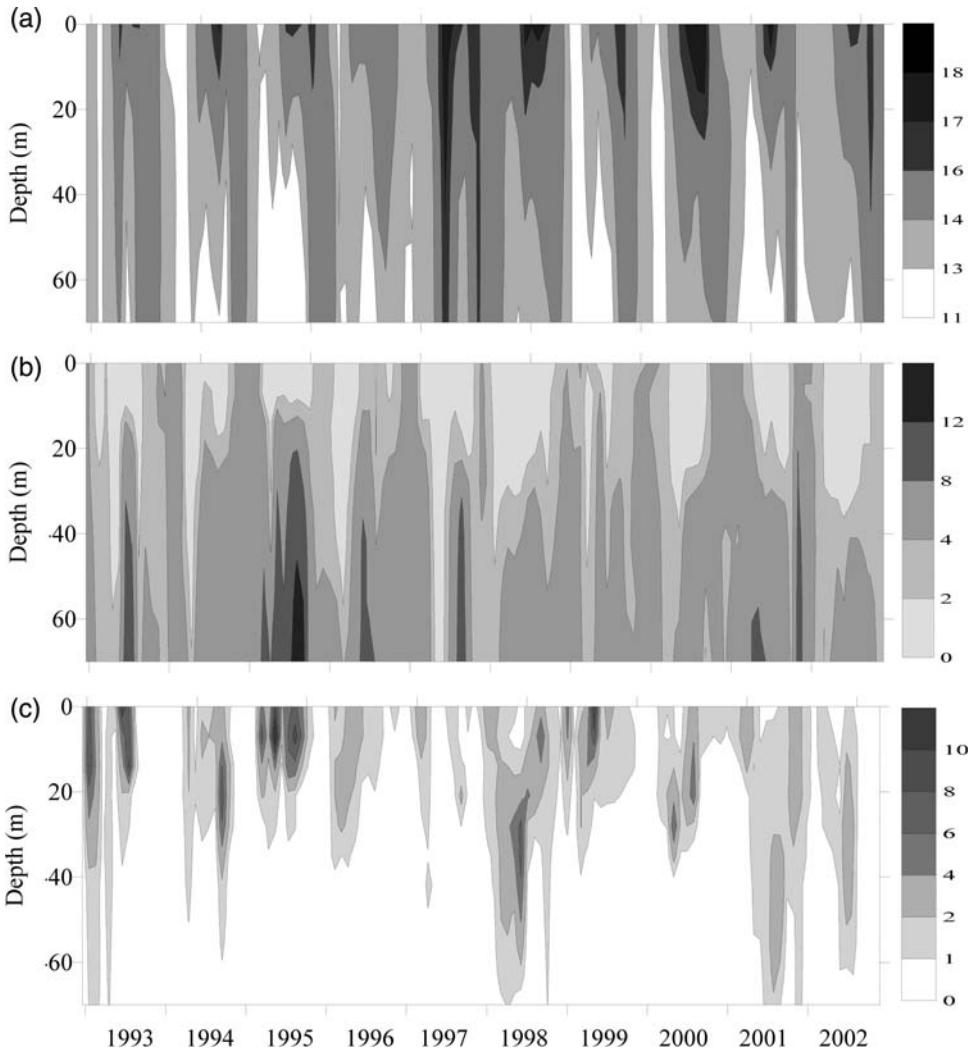

Fig. 3. Temporal and vertical variability in (a) temperature (°C), (b) nitrate concentration (μmol L^{-1}) and (c) Chl *a* concentration (mg m^{-3}).

structure. In contrast, a higher variability in slope values was observed during the stratification period. In this case, more negative values were registered in surface waters and less negative values appeared below the depth of 20 m, indicating an increasing importance of larger phytoplankton in deeper waters.

Finally, we tried to ascertain whether or not there was any relationship between phytoplankton biomass, as represented by Chl *a* concentration, and the parameters of the scaling relationship between abundance and cell size. We classified all the sampling dates into three groups, according to the values of surface Chl *a* concentration: <0.2, $0.2-2$ and >2 mg Chl *a* m^{-3}. Size–abundance macrospectra were then constructed for each group by plotting together all the water column macrospectra corresponding to each chlorophyll level. The slope of the high chlorophyll macrospectrum (-0.93) was significantly less negative (Clarke test, $P<0.001$) than that of the low chlorophyll macrospectrum (-0.97), indicating a higher relative importance of larger cells during conditions of high phytoplankton biomass (Table III). In contrast, no significant differences were found between the medium chlorophyll macrospectrum and the other chlorophyll macrospectra (Clarke test, $P>0.05$). In addition, the intercept of the low chlorophyll macrospectrum had a significantly lower value, reflecting a lower phytoplankton abundance in all size classes when compared with the other two situations. In contrast, the high chlorophyll macrospectrum showed the highest value of the intercept, corresponding to the highest abundance levels.

Time-series analysis

The temporal variation in the slope of the water column macrospectra, together with the slopes of the 5

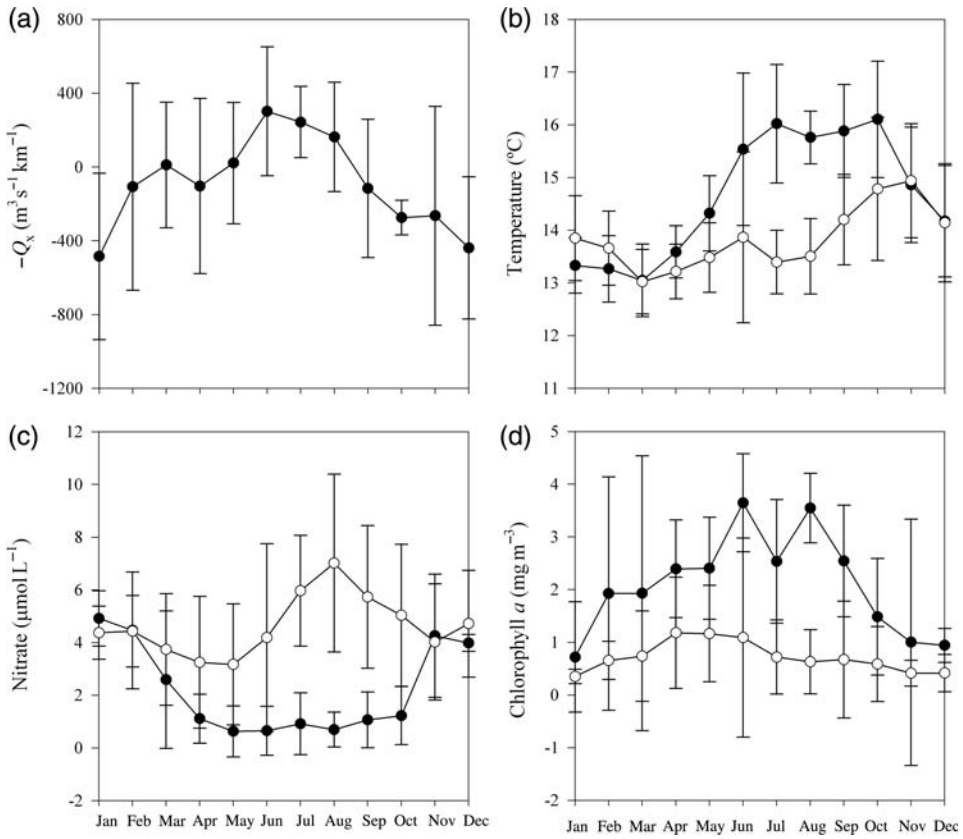

Fig. 4. Monthly mean values of (a) upwelling index (m^3 s^{-1} km^{-1}), (b) temperature (°C), (c) nitrate concentration (μmol L^{-1}) and (d) Chl *a* concentration (mg m^{-3}). In (b–d), filled circles correspond to 5 m depth values and open circles to 40 m depth values. Error bars indicate ± 1 SD.

Table I: Characteristics of the different hydrographic periods identified for the 10-year time series

Hydrographic period	*n*	Temperature	Nitrate	Brunt–Väisälä frequency	Chl *a*	Ekman transport
Winter mixing	41	13.8 (0.8)	3.9 (1.8)	0.003	1.0 (0.9)	−388
Upwelling type I	12	14.0 (1.5)	2.2 (2.4)	0.003	1.8 (3.1)	434
Upwelling type II	20	14.2 (1.4)	1.1 (1.2)	0.005	2.4 (1.1)	312
Stratification	23	15.9 (1.0)	0.8 (0.9)	0.013	2.5 (2.6)	50
Downwelling	11	16.4 (0.8)	1.8 (1.2)	0.008	1.8 (2.4)	−624

Shown are mean surface values (5 m depth) for temperature (°C), nitrate concentration (μmol L^{-1}) and Chl *a* concentration (mg m^{-3}). *n* indicates the number of stations included in each period. Brünt–Väisäla frequency was calculated between 0 and 40 m of depth. Ekman transport (m^3 s^{-1} km^{-1}) was averaged over the 6 days prior to sampling date. Standard deviation for each variable is in parentheses.

and 40 m depth size–abundance spectra for the entire time series, are shown in Fig. 8. We observed a significant trend towards less negative slopes in all three variables (trend slope = 0.014, $P < 0.05$ for water column macrospectra slopes, trend slope = 0.015, $P < 0.05$ for 5 m depth spectra slopes and trend slope = 0.015, $P < 0.01$ for 40 m depth spectra slopes). In order to determine whether these interannual trends were due to an increase in the abundance of larger cells or a reduction in the abundance of smaller species, we examined the temporal evolution in the biovolume of the three main phytoplankton groups, namely flagellates (2–9 μm ESD), dinoflagellates (7–72 μm ESD) and diatoms (3–230 μm ESD) (data not shown). Only the flagellates showed a significant change in biovolume during the study, with lower values towards the end of the sampling period ($P < 0.001$ at 5 m and < 0.05 at 40 m depth). We also found a significant, negative correlation between flagellate biovolume at a depth of 5 and 40 m and the spectral slopes at these depths ($r^2 = 0.23$, $P < 0.05$; $r^2 = 0.19$, $P < 0.05$, respectively). It thus seems that the temporal trend towards less negative slopes in the size–abundance relationship (e.g. an increase in the relative importance of larger cells) would result from a decrease

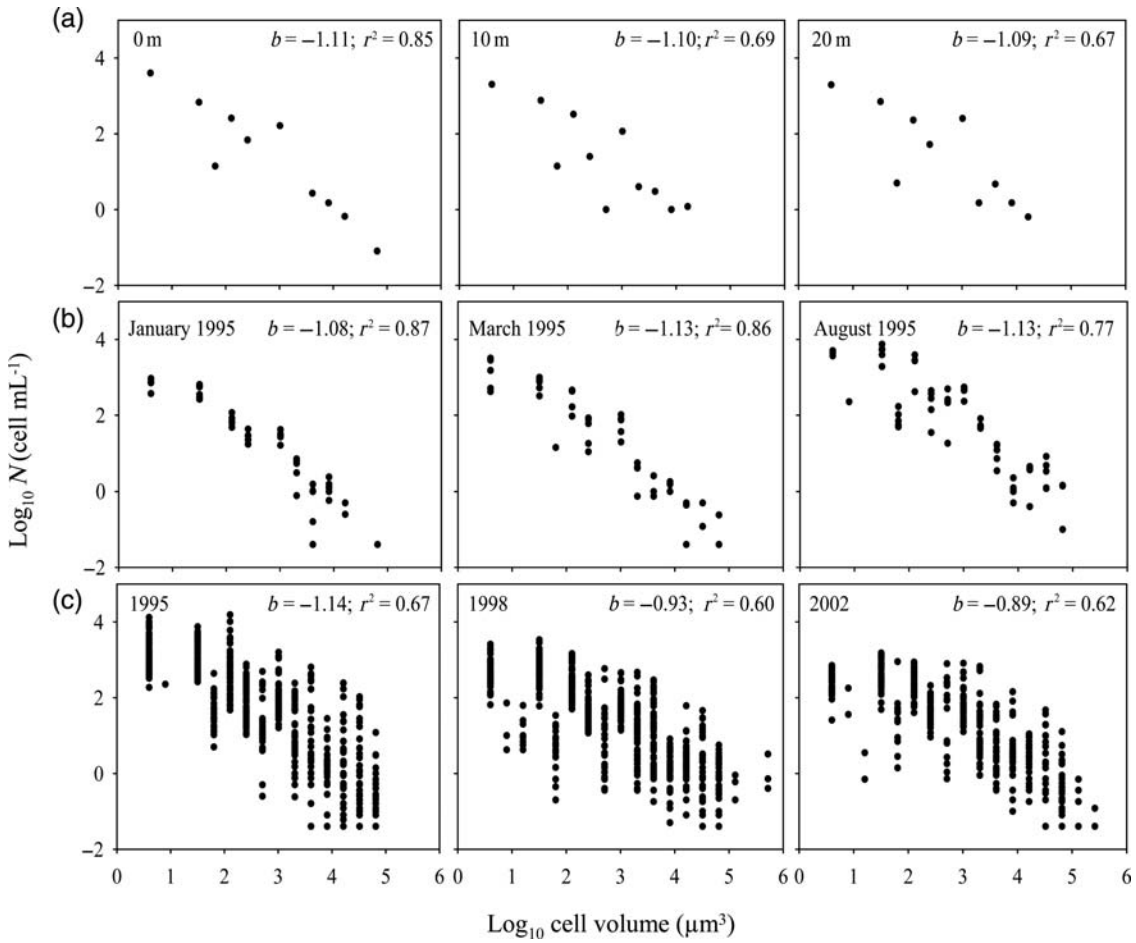

Fig. 5. Representative abundance–size spectra at different levels of integration: (a) abundance–size spectra at different depths on a particular sampling day (November 16, 1994), (b) water-column abundance–size macrospectra for January 1995, March 1995 and August 1995 and (c) abundance–size macrospectra for 1995, 1998 and 2002. Each spectrum was fitted to a linear model by r.m.a. regression.

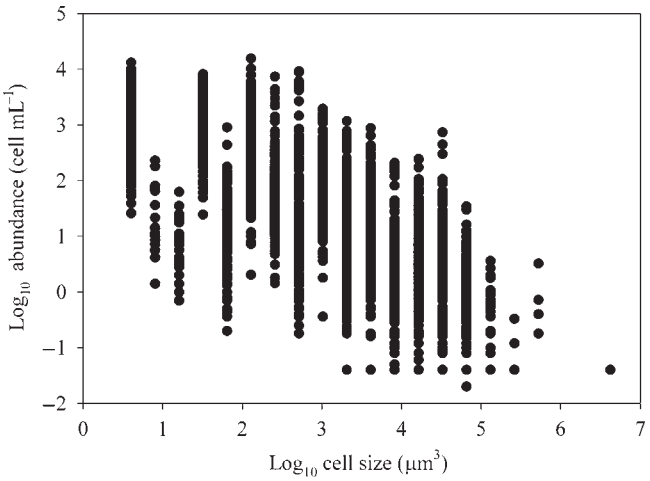

Fig. 6. Overall size–abundance macrospectrum for the whole time series. The regression line is: $\log_{10}$ total abundance = 4.12–0.97 $\log_{10}$ cell size ($r^2 = 0.59$; $P < 0.0001$, $n = 5964$).

Table II: Statistical parameters for the relationship between log_{10} total cell abundance and log_{10} nominal size for the different hydrographic periods analysed during 1993–2002

Hydrographic period	*n*	*Y*-intercept	*b* (slope)	r^2
Winter mixing	2107	3.92 (3.85, 4.00)	−0.97 (−0.99, −0.95)	0.65
Upwelling type I	669	4.22 (4.07, 4.38)	−0.98 (−1.03, −0.94)	0.58
Upwelling type II	1066	4.05 (4.05, 4.16)	−0.85 (−0.88, −0.82)	0.50
Stratification	1188	4.35 (4.24, 4.47)	−0.99 (−1.03, −0.96)	0.60
Downwelling	470	4.11 (3.96, 4.27)	−1.01 (−1.05, −0.96)	0.68

The *Y*-intercept and slope (*b*) were obtained using r.m.a. regression analysis. *n* indicates the number of observations included into the regression analysis. Confidence limits (95%) for the intercept and slope are given in parentheses.

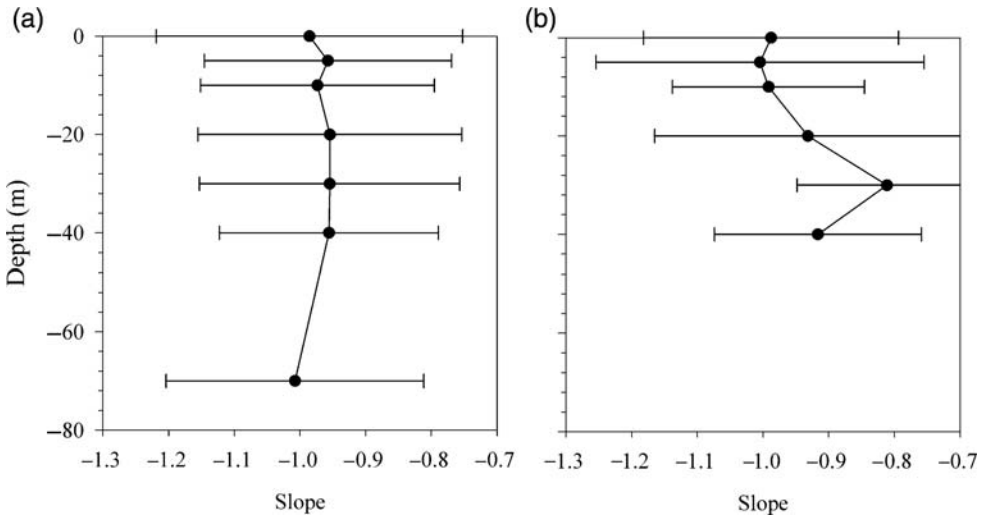

Fig. 7. Vertical variability of the mean macrospectrum slopes during (a) winter mixing and (b) summer stratification.

Table III: Statistical parameters of the macrospectra obtained with samples of different levels of Chl a *concentration (mg m^{-3})*

Chl *a*	*n*	*Y*-intercept	*b* (slope)	r^2
<0.2 mg m^{-3}	2349	3.89 (3.83, 3.86)	−0.97 (−0.99, −0.95)	0.70
0.2–2 mg m^{-3}	1440	4.08 (3.98, 4.18)	−0.95 (−0.98, −0.92)	0.59
>2 mg m^{-3}	1936	4.27 (4.18, 4.36)	−0.93 (−0.95, −0.90)	0.52

The *Y*-intercept and slope (*b*) were obtained using reduced major axis regression analysis. *n* indicates the number of observations included into the regression analysis. Confidence limits (95%) for the intercept and slope are given in parentheses.

in flagellate biomass rather than an increase in the biomass of diatoms or dinoflagellates.

In order to explore the possible causes for the observed interannual trends in the size–abundance slope and the biomass of flagellates, we analysed the temporal variability in sea surface temperature and salinity, nutrient concentration at 5 and 40 m depth, mixing layer depth, Ekman transport and North Atlantic Oscillation index, as well as their cross-correlation with the phytoplankton size structure. However, we did not find any significant correlation between the slope of the size–abundance spectrum (calculated both on an annual and a monthly basis) and these hydrographic and climatic variables. On the contrary, when we analysed separately the relationship between deseasonalized flagellate biovolume and deseasonalized hydrographic variables, we found that the biomass of this phytoplankton group was inversely correlated with mixing layer depth. This means that, when mixing depth was shallower (and, therefore, water-column stratification was more intense), flagellates tended to be more abundant.

DISCUSSION

General patterns in the size scaling of phytoplankton abundance

Although several studies have previously addressed the temporal (Gilabert, 2001; Reul *et al.*, 2005) and vertical (Gin *et al.*, 1999, Rodríguez *et al.*, 2001) variability in the size scaling of phytoplankton abundance in marine

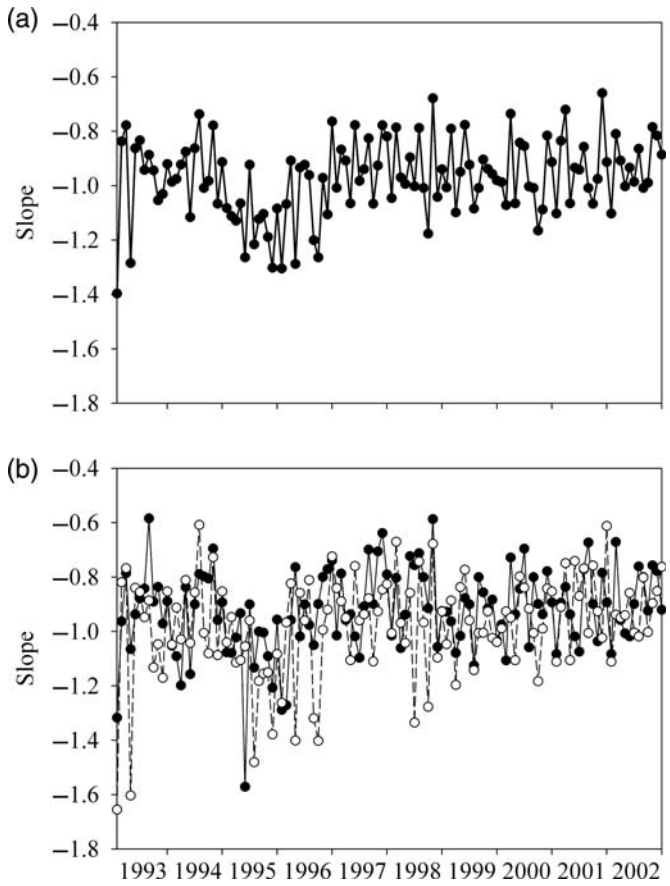

Fig. 8. Temporal evolution in the slope of (a) water-column macrospectra and (b) spectra from 5 m (white circle, dashed line) and 40 m (dark circle, solid line) depths.

ecosystems, to our knowledge this is the first study that includes repeated monthly observations over both seasonal and interannual time scales. The present work thus provides a robust description of general patterns in the phytoplankton size structure of coastal waters, which is based on the analysis of some 600 size–abundance spectra. Our data indicate that the linear inverse relationship between abundance and cell size (i) is persistent throughout the water column and across seasonal and interannual time scales and (ii) can be adequately described by a power law.

It has been often emphasized that more productive ecosystems subjected to stronger hydrodynamic forcing can show departures (i.e., dome-like patterns) in the linear relationship between abundance and cell size (Sprules and Munawar, 1986; Dickie *et al.*, 1987), as blooms of one or a few species would cause a significant departure from linearity in the log–log relationship between abundance and cell size (e.g. Reul *et al.*, 2006). In our study, however, even though more than 10-fold changes in phytoplankton chlorophyll were observed over seasonal time scales, the size-scaling relationship could be always adequately described by a statistically significant regression line and major departures from linearity were seldom observed (Fig. 5). Recent modelling work has shown that the power-law relationship between abundance and cell size results from the size scaling of cellular nutrient requirements and growth (Irwin *et al.*, 2006), without the need to invoke other mechanisms such as competition or size-dependent changes in grazing and sedimentation. Although the precise parameters of the functions relating cell size to resource use and growth rate change according to taxonomic affiliation and resource availability, among other factors (Banse, 1982; Finkel, 2001; Marañón *et al.*, 2007), these relationships tend to conform to a power law. This explains our observation that the scaling of phytoplankton abundance and cell size, even in a productive ecosystem, can also be described by a power relationship, and the persistence of this relationship throughout the study and at different levels of integration suggests the importance of bottom-up control of the phytoplankton size structure in the study site.

The scaling of phytoplankton abundance and cell size depends on resource availability: less productive

waters are characterized by steeper (more negative) slopes, indicating a higher relative importance of smaller species (Gin *et al.*, 1999; Cavender-Bares *et al.*, 2001; Marañón *et al.*, 2007). Cermeño and Figueiras (Cermeño and Figueiras, 2008) provided a review of size spectra for nano- and micro-phytoplankton obtained in regions of contrasting trophic status (their Table 1). They found that the slope of the size spectrum ranged from values around -0.8 in coastal, eutrophic ecosystems (where mean primary production over the year is usually higher than 2 gC m^{-2} day^{-1}) to values as low as -1.3 for the ultra-oligotrophic waters of the Atlantic subtropical gyres (where typical primary production rates are below 0.3 g C m^{-2} day^{-1}). The average slope observed in the present study (-0.96) agrees with the fact that our study site is characterized by high productivity (mean primary production over the period 1993–2002 was 1.7 g C m^{-2} day^{-1}). In Ría de Vigo, a coastal embayment which is located some 150 km to the south of our study site and has an average primary production of ca. 2.5 g C m^{-2} day^{-1} (Marañón *et al.*, 2004; Cermeño *et al.*, 2006), the slope of the phytoplankton size spectra takes values between -0.9 and -0.8 (Marañón *et al.*, 2007; Cermeño and Figueiras, 2008). These results illustrate the macroecological pattern whereby increasingly productive regions tend to show an increasing dominance by larger phytoplankton (Chisholm, 1992; Marañón *et al.*, 2001; Marañón, 2009).

Our observations of the scaling between cell size and abundance have direct implications for the distribution of phytoplankton biomass along the size spectrum. If phytoplankton total abundance (N) scales with cell size (M) according to $N \propto M^b$ and phytoplankton carbon biomass per cell (C) scales with M as $C \propto M^c$, then total biomass ($N \times C$) will scale as M^{b+c}. Although the determination of the value of c is subject to several methodological uncertainties, most recent estimates fall in the range 0.9–1 (Montagnes and Berges, 1994; Menden-Deuer and Lessard, 2000; Finkel, 2001), which implies that, for our study system, $b + c$ will take an average value close to zero. This would mean that, within the nano- to micro-phytoplankton size range, approximately equal amounts of biomass are contained within each logarithmic size class. This result is in accordance with the early observations of Sheldon *et al.* (Sheldon *et al.*, 1972), although in their case biovolume rather than biomass was considered.

Hydrography and phytoplankton size structure

With the exception of the upwelling relaxation phase, we found that size macrospectra had similar slopes in the different hydrographic conditions identified (Table II). This suggests that, under these oceanographic conditions, both nano- and micro-phytoplankton respond similarly to changes in hydrodynamic forcing and resource availability. Similar observations have been reported for the southern Bay of Biscay, where the slopes of size spectra of seston particle biovolume exhibited low variability, despite a large range of Brunt–Väisalä values observed during the seasonal cycle (Bode and Fernández, 1992). Although the spectra constructed by Bode and Fernández (Bode and Fernández, 1992) were normalized biomass size spectra, the direct comparison with our slope values is possible, as the regression parameters of both scaling approaches are equivalent (Blanco *et al.*, 1994). In addition, in the Galician shelf, the biomass of both nanoplankton and microplankton increased similarly (by a factor of 2) from winter to spring bloom conditions (Bode *et al.*, 1994). Lower standing stocks of phytoplankton in winter, which result from excessive mixing and low light availability, are also reflected in our analysis, since the winter size macrospectra had a significantly lower Y-intercept than those of the stratification and upwelling periods (Table II).

Upwelling relaxation (defined as upwelling II in our analysis) brings about the largest increases in phytoplankton biomass and productivity in the Galician Rías and shelf (Bode and Varela, 1994; Casas *et al.*, 1999; Tilstone *et al.*, 2000). During the peak of the upwelling event, when upward water velocities are highest, relatively strong turbulence and offshore wash-out of cells, together with the physiological time lag required for communities to adjust to the new conditions, prevent the accumulation of large amounts of phytoplankton. During upwelling relaxation, however, high nutrient concentrations combined with enhanced water-column stability and reduced dispersion allow the onset of phytoplankton blooms, which are typically dominated by chain-forming diatoms. In our study, this process is shown in a significantly less negative slope (-0.85) of the size macrospectrum (Table II), which indicates the increasing dominance of larger cells. The common association between increased phytoplankton biomass and productivity and a higher dominance of large phytoplankton, and in particular diatoms, has been often attributed to trophic effects (Kiørboe, 1993; Irigoien *et al.*, 2005). In this view, large phytoplankton dominance is not caused by higher intrinsic growth rates, relative to those of smaller phytoplankton, but rather from the higher grazing pressure experienced by the latter. However, there is recent evidence, both from modelling (Irwin *et al.*, 2006) and experimental studies (Cermeño *et al.*, 2005; Marañón *et al.*, 2007), which

suggests that large phytoplankton are capable of sustaining higher growth rates than small phytoplankton under conditions of high resource availability.

Our observations also allow us to extract some conclusions regarding the vertical variability in phytoplankton size structure (Fig. 7). During the winter-mixing period, the slope of the size spectrum was constant with depth, reflecting a relatively homogeneous size structure throughout the euphotic layer. However, during the stratification period the slope became less negative with depth (-0.8 at 30 m compared with -1 at the surface), which indicates that the relative importance of large phytoplankton was greater near the bottom of the euphotic layer. This pattern contrasts with that reported for the stratified waters of the tropical and subtropical open ocean, where the deep chlorophyll maximum (DCM) is characterized by an increased dominance of small phytoplankton, compared with the upper mixed layer (Gin *et al.*, 1999; Pérez *et al.*, 2006; Poulton *et al.*, 2006). These authors have interpreted this pattern as a result of the higher light-use efficiency of smaller cells, which would be advantageous in the low-irradiance conditions of the bottom of the euphotic layer. It has to be noted, however, that the DCM in the low-latitude open ocean is a permanent structure characteristic of a near steady-state ecosystem. In our study site, a coastal location subject to intermittent upwelling during summer, stratification is never a persistent feature as it is in the typical temperate zones, but rather appears only between successive upwelling pulses. After each upwelling-caused bloom, intense sedimentation of large, fast-sinking species takes place (Figueiras and Pazos, 1991; Varela *et al.*, 1991; Cermeño *et al.*, 2006), which explains the observed trend towards less negative size spectrum slopes in subsurface waters. In contrast, the surface layer, where nutrients are scarcer, is dominated by smaller species (Varela *et al.*, 1991), which are better adapted to use low concentrations of nutrients (Chisholm, 1992; Kiørboe, 1993).

Interannual variability in size spectra

Although longer time series are needed in order to establish significant, long-term trends in the structure and functioning of marine ecosystems (e.g. Leterme *et al.*, 2005), our data set allowed us to explore the interannual variability in phytoplankton size structure, as represented by the parameters of the size spectra during a 10-year period. We found that community size structure showed a significant interannual trend towards less negative slope values (Fig. 8). Although there was no significant correlation between the slope of the size spectrum and the interannual variability in the physico-chemical variables, we did find that the observed trend in slope was related to a decrease in flagellate abundance, rather than to any change in the abundance of diatoms or dinoflagellates. Moreover, the biomass of flagellates (<10 μm in ESD) was inversely correlated to the mixing layer depth, which would suggest that in more stratified settings flagellates are favoured relative to other phytoplankton groups. As mentioned above, the association between enhanced stratification, reduced nutrient supply and increased dominance of small cells is a well-established pattern in biological oceanography (Chisholm, 1992; Kiørboe, 1993). Additional studies are required, however, to ascertain the occurrence and causal mechanisms of interannual trends in the composition and size structure of phytoplankton in our study region.

CONCLUSIONS

Even though our study ecosystem is highly productive and characterized by marked temporal changes in hydrodynamics, the inverse linear relationship between phytoplankton abundance and cell size was persistent over seasonal and interannual time scales. In addition, it could be adequately described by a power-law model, which makes it easy to incorporate into size-based mathematical models of plankton dynamics. The slope of the size macrospectrum obtained from the overall time series had a value of -0.96, which indicates that roughly equal amounts of biomass were present over the different logarithmic size classes in the nano- to micro-phytoplankton size range. During the different hydrographic periods that occur over the year, the slope of the size macrospectrum had a similar value, suggesting that both the nanophytoplankton and the microphytoplankton often respond similarly to environmental forcing. An exception was the upwelling relaxation period, when a stronger dominance of large phytoplankton resulted in a significantly less negative (-0.85) slope. The vertical variability in the size spectrum slope during stratification showed a trend towards less negative values with depth, probably as a result of sedimentation of large cells after an upwelling-caused bloom. Our results illustrate the utility of individual size distributions to provide a synthetic description of phytoplankton community structure in dynamic, non-steady-state marine ecosystems.

FUNDING

This research was funded by the Spanish Ministerio de Ciencia e Innovación (MICINN) through grant

CTM2008-03699 (Macroecological patterns in marine phytoplankton) to E.M., as well as by the Instituto Español de Oceanografía through their programme RADIALES. M.H.-O. was supported by an undergraduate FPU fellowship from MICINN.

ACKNOWLEDGEMENTS

We thank P. Cermeño for his useful comments and J. L. Herrera-Cortijo for his advice on time-series analysis. G.G.-N. and E. N. kindly provided the software subroutines for statistical time-series analysis. Comments from two anonymous reviewers are also gratefully acknowledged.

REFERENCES

Azam, F., Fenchel, T., Field, J. G. *et al.* (1983) The ecological role of water-column microbes in the sea. *Mar. Ecol. Prog. Ser.*, **10**, 257–263.

Banse, K. (1982) Cell volumes, maximal growth rates of unicellular algae and ciliates, and the role of ciliates in the marine pelagial. *Limnol. Oceanogr.*, **27**, 1059–1071.

Blanco, J. M., Echevarría, F. and García, C. M. (1994) Dealing with size spectra: some conceptual and mathematical problems. In Rodríguez, J. and Li, W. K. W. (eds), *The Size Structure and Metabolism of the Pelagic Ecosystems. Sci. Mar.*, **58**, 17–29.

Bode, A. and Fernández, E. (1992) Influence of water-column stability on phytoplankton size and biomass sucession patterns in the central Cantabrian Sea (Bay of Biscay). *J. Plankton Res.*, **14**, 885–902.

Bode, A. and Varela, M. (1994) Planktonic carbon and nitrogen budgets for the N-NW Spanish shelf: The role of pelagic nutrient regeneration during upwelling events. *Sci. Mar.*, **58**, 221–231.

Bode, A., Casas, B. and Varela, M. (1994) Size-fractionated primary productivity and biomass in the Galician shelf (NW Spain): netplankton versus nanoplankton dominance. In Rodríguez, J. and Li, W. K. W. (eds), *The Size Structure and Metabolism of the Pelagic Ecosystems. Sci. Mar.*, 58, 131–141.

Brown, J. H., Gillooly, J. F., Allen, A. P. *et al.* (2004) Toward a metabolic theory of ecology. *Ecology*, **85**, 1171–1789.

Casas, B., Varela, M., Canle, M. *et al.* (1997) Seasonal variations of nutrients, seston and phytoplankton, and upwelling intensity off La Coruña (NW Spain). *Estuarine Coastal Shelf Sci.*, **44**, 767–778.

Casas, B., Varela, M. and Bode, A. (1999) Seasonal succession of phytoplankton species on the coast of A Coruña (Galicia, northwest Spain). *Bol. Inst. Esp. Oceanogr.*, **15**, 413–429.

Cavender-Bares, K., Rinaldo, A. and Chisholm, S. W. (2001) Microbial size spectra from natural and nutrient enriched ecosystems. *Limnol. Oceanogr.*, **46**, 778–789.

Cermeño, P. and Figueiras, F. G. (2008) Species richness and cell-size distribution: the size structure of phytoplankton communities. *Mar. Ecol. Prog. Ser.*, **357**, 79–85.

Cermeño, P., Marañón, E., Rodríguez, J. *et al.* (2005) Large-sized phytoplankton sustain higher carbon-specific photosynthesis than smaller cells in a coastal eutrophic ecosystem. *Mar. Ecol. Prog. Ser.*, **297**, 51–60.

Cermeño, P., Marañón, E., Pérez, V. *et al.* (2006) Phytoplankton size structure and primary production in a highly dynamic coastal ecosystem (Ría de Vigo, NW Spain): Seasonal and short-time variabiliy. *Estuarine Coastal Shelf Sci.*, **67**, 251–266.

Chisholm, S. W. (1992) Phytoplankton size. In Falkowski, P. G. and Woodhead, A. D. (eds), *Primary Productivity and Biogeochemical Cycles in the Sea*. Plenum Press, New York, pp. 213–236.

Clarke, M. R. B. (1980) The reduced major axis of a bivariate sample. *Biometrika*, **67**, 441–446.

Cushing, D. H. (1989) A difference in structure between ecosystems in strongly stratified waters and in those that are only weakly stratified. *J. Plankton Res.*, **11**, 1–13.

Dickie, L. M., Kerr, S. R. and Boudreau, P. R. (1987) Size-dependent processes underlying regularities in ecosystem structure. *Ecol. Monogr.*, **57**, 233–250.

Edler, L. (1979) Recommendations for marine biological studies in the Baltic Sea. Phytoplankton and Chlorophyll. *Baltic Mar. Biol. Publ.*, **5**, 1–38.

Figueiras, F. G. and Pazos, Y. (1991) Hydrography and phytoplankton of the Ría de Vigo before and during a red tide of *Gymnodinium catenatum.* Graham. *J. Plankton Res.*, **13**, 589–608.

Finkel, Z. V. (2001) Light absorption and size scaling of light-limited metabolism in marine diatoms. *Limnol. Oceanogr.*, **46**, 86–94.

Fraga, F. (1981) Upwelling off the Galician Coast. In Richards, F. A. (ed), *Upwelling Ecosystems*. American Geophysical Union, Washington, pp. 176–182.

Gilabert, J. (2001) Short-term variability of the planktonic size structure in a Mediterranean coastal lagoon. *J. Plankton Res.*, **23**, 219–226.

Gin, K. Y. H., Chisholm, S. W. and Olson, R. J. (1999) Seasonal and depth variation in microbial size spectra at the Bermuda Atlantic time series station. *Deep-Sea Res. I*, **46**, 1221–1245.

Irigoien, X., Flynn, K. J. and Harris, R. P. (2005) Phytoplankton blooms: a "loophole" in microzooplankton grazing impact? *J. Plankton Res.*, **27**, 313–321.

Irwin, A., Finkel, Z. V., Schofield, O. M. E. *et al.* (2006) Scaling-up from nutrient physiology to the size-structure of phytoplankton communities. *J. Plankton Res.*, **28**, 459–471.

Kiørboe, T. (1993) Turbulence, phytoplankton cell size and the structure of pelagic food webs. *Adv. Mar. Biol.*, **29**, 1–72.

Lavin, A., Díaz del Río, G., Cabanas, J. M. *et al.* (1991) Afloramiento en el noroeste de la Península Ibérica. Indices de afloramiento para el punto 43°N 11°W: Período 1966–1989. *Inf. Téc. Inst. Esp. Oceanog*, **91**, 1–40.

Laws, E. A. and Archie, J. W. (1981) Appropriate use of regression analysis in marine biology. *Mar. Biol.*, **65**, 1432–1793.

Legendre, L. and Rassoulzadegan, F. (1996) Food-web mediated export of biogenic carbon in oceans: hydrodinamic control. *Mar. Ecol. Prog. Ser.*, **145**, 179–193.

Leterme, S. C., Edwards, M., Seuront, L. *et al.* (2005) Decadal basin-scale in diatoms, dinoflagellates, and phytoplankton color across the North Atlantic. *Limnol. Oceanogr.*, **50**, 1244–1253.

Lund, J. W. G., Kipling, C. and Le Cren, E. D. (1958) The inverted microscope method of estimating algal numbers and the statistical basis of estimations by counting. *Hydrobiologia*, **11**, 143–170.

Marañón, E. (2009) Phytoplankton size structure. In Steele, J. H., Turekian, K. K. and Thorpe, S. A. (eds), *Encyclopedia of Ocean Sciences*. Academic Press, Oxford, pp. 4252–4256.

Marañón, E., Holligan, P. M., Barciela, R. *et al.* (2001) Patterns of phytoplankton size-structure and productivity in contrasting open ocean environments. *Mar. Ecol. Prog Ser.*, **216**, 43–56.

Marañón, E., Cermeño, P., Fernández, E. *et al.* (2004) Significance and mechanisms of photosynthetic production of dissolved organic carbon in a coastal eutrophic ecosystem. *Limnol. Oceanogr.*, **49**, 1652–1666.

Marañón, E., Cermeño, P., Rodríguez, J. *et al.* (2007) Scaling of phytoplankton photosynthesis and cell size in the ocean. *Limnol. Oceanogr.*, **52**, 2190–2198.

Menden-Deuer, S. and Lessard, E. J. (2000) Carbon to volume relationships for dinoflagellate, diatoms, and other protist plankton. *Limnol. Oceanogr.*, **45**, 569–579.

Montagnes, D. J. S. and Berges, J. A. (1994) Estimating carbon, nitrogen, protein, and chlorophyll *a* from volume in marine phytoplankton. *Limnol. Oceanogr.*, **39**, 1044–1060.

Nogueira, E., Pérez, P. P. and Ríos, A. F. (1997) Seasonal patterns and long-term trends in an estuarine upwelling ecosystem (Ría de Vigo, NW Spain). *Estuarine Coastal Shelf Sci.*, **44**, 285–300.

Pérez, V., Fernández, E., Marañón, E. *et al.* (2006) Vertical variability of phytoplankton biomass, production and growth in the Atlantic subtropical gyres. *Deep-Sea Res. I*, **53**, 1616–1634.

Peters, R. H. (1983) *The Ecological Implications of Body Size*. Cambridge University Press, Cambridge.

Poulton, A. J., Holligan, P. M., Hickman, A. *et al.* (2006) Phytoplankton carbon fixation, chlorophyll-biomass and diagnostic pigments in the Atlantic Ocean. *Deep-Sea Res. II*, **53**, 1593–1610.

Reul, A., Rodríguez, V., Jiménez-Gómez, F. *et al.* (2005) Variability in the spatio-temporal distribution and size-structure of phytoplankton across an upwelling area in the NW-Alboran Sea, (W-Mediterranean). *Cont. Shelf Res.*, **25**, 589–608.

Reul, A., Rodríguez, J., Blanco, J. M. *et al.* (2006) Control of microplankton size structure in contrasting water columns of the Celtic Sea. *J. Plankton Res.*, **28**, 449–457.

Rodríguez, J. and Mullin, M. M. (1986) Relation between biomass and body weight of plankton in a steady state oceanic ecosystem. *Limnol. Oceanogr.*, **31**, 361–370.

Rodríguez, J., Jimenez, F., Bautista, B. *et al.* (1987) Planktonic biomass spectra dynamics during a winter production pulse in Mediterranean coastal waters. *J. Plankton Res.*, **9**, 1183–1194.

Rodríguez, J., Tintoré, J., Allen, J. T. *et al.* (2001) Mesoscale vertical motion and the size structure of phytoplankton in the ocean. *Nature*, **410**, 360–363.

Sheldon, R. W., Prakash, A. and Sutcliffe, W. H. (1972) The size distribution of particles in the ocean. *Limnol. Oceanogr*, **17**, 327–340.

Sprules, W. G. and Munawar, M. (1986) Plankton size spectra on relation to ecosystem productivity, size and perturbation. *Can. J. Fish. Aquat. Sci.*, **43**, 1789–1794.

Teira, E., Abalde, J., Alvarez-Ossorio, M. *et al.* (2003) Plankton carbon budget in a coastal wind-driven upwelling station off A Coruña (NW Iberian Peninsula). *Mar. Ecol. Prog Ser.*, **265**, 31–43.

Tilstone, G. H., Míguez, B. M., Figueiras, F. G. *et al.* (2000) Diatom dynamics in a coastal ecosystem affected by upwelling: coupling between species succession, circulation and biogeochemical processes. *Mar. Ecol. Prog Ser.*, **205**, 23–41.

Valdés, L., Lavín, A., Fernández de Puelles, M. L. *et al.* (2002) Spanish Ocean Observation System. IEO Core Project: studies on time series of oceanographic data. In Flemming, N. C., Vallerga, S., Pinardiet, N. *et al.* (eds), *Operational Oceanography: Implementation at the European and regional Scales*. Elsevier Science B. V, Amsterdam, pp. 99–105.

Varela, M., del Río, G., Alvarez-Ossorio, M. *et al.* (1991) Factors controlling phytoplankton size class distribution in the upwelling area of the Galician continental shelf (NW Spain). *Sci. Mar.*, **55**, 505–518.

Varela, M., Prego, R., Belzunce, M. J. *et al.* (2001) Inshore-offshore differences in seasonal variations of phytoplankton assemblanges: the case of a Galician Ria Alta (A Coruña Ria) and its adjacent shelf (NW Spain). *Cont. Shelf Res.*, **21**, 1815–1838.

White, E. P., Ernest, S. K. M., Kerkhoff, A. J. *et al.* (2007) Relationships between body size and abundance in ecology. *Trends Ecol. Evol.*, **22**, 323–330.